European Radiology (2021) 31:5669–5679
https://doi.org/10.1007/s00330-021-07705-3

MAGNETIC RESONANCE

Evaluation of microvascular permeability of skeletal muscle and texture analysis based on DCE-MRI in alloxan-induced diabetic rabbits

Baiyu Liu[1] · Lei Hu[1] · Li Wang[1] · Dong Xing[1] · Lin Peng[1] · Pianpian Chen[1] · Feifei Zeng[1] · Weiyin Vivian Liu[2] · Huan Liu[3] · Yunfei Zha[1]

Received: 20 February 2020 / Revised: 24 November 2020 / Accepted: 21 January 2021 / Published online: 5 February 2021

Abstract

Objectives To estimate the microvascular permeability and perfusion of skeletal muscle by using quantitative dynamic contrast-enhanced magnetic resonance imaging (DCE-MRI) and explore the feasibility of using texture analysis (TA) to evaluate subtle structural changes of diabetic muscles.

Methods Twenty-four rabbits were randomly divided into diabetic (n = 14) and control (n = 10) groups, and underwent axial DCE-MRI of the multifidus muscle (0, 4, 8, 12, and 16 weeks after alloxan injection). The pharmacokinetic model was used to calculate the permeability parameters; texture parameters were extracted from volume transfer constant (K^{trans}) map. The two-sample t test/Mann-Whitney U test, repeated measures analysis of variance/Friedman test, and Pearson correlations were used for data analysis.

Results In the diabetic group, K^{trans} and rate constant (K_{ep}) increased significantly at week 8 and then showed a decreasing trend. Extravascular extracellular space volume fraction (V_e) increased and plasma volume fraction (V_p) decreased significantly from the 8th week. Skewness began to decrease at the 4th week. Median K^{trans} and entropy increased significantly, while inverse difference moment decreased from the 8th week. Energy decreased while contrast increased only at week 8. Muscle fibre cross-sectional area was negatively correlated with V_e. The capillary-to-fibre ratio was positively correlated with V_p ($p < 0.05$, all).

Conclusions Quantitative DCE-MRI can be used to evaluate microvascular permeability and perfusion in diabetic skeletal muscle at an early stage; TA based on K^{trans} map can identify microarchitectural modifications in diabetic muscles.

Key Points

- *Four quantitative parameters of DCE-MRI can be used to evaluate microvascular permeability and perfusion of skeletal muscle in diabetic models at early stages.*
- *Texture analysis based on K^{trans} map can identify subtle structural changes in diabetic muscles.*

Keywords Diabetes mellitus · Muscles · Magnetic resonance imaging · Permeability · Perfusion

Abbreviations

AIF	Arterial input function
ASL	Arterial spin labelling
ASM	Angular second moment
C/F	Capillary-to-fibre
CEU	Contrast-enhanced ultrasound
CSA	Cross-sectional area
DCE-MRI	Dynamic contrast-enhanced magnetic resonance imaging
DM	Diabetes mellitus
DSC	Dynamic susceptibility contrast
EES	Extravascular extracellular space
FOV	Field of view
GLCM	Grey level co-occurrence matrix
HE	Haematoxylin-eosin
I/R	Ischaemia-reperfusion
$IAUC_{60}$	Initial area under the signal intensity-time curve value over the first 60 s

✉ Yunfei Zha
zhayunfei999@126.com

[1] Department of Radiology, Renmin Hospital of Wuhan University, Wuhan 430060, China

[2] MR Research, GE Healthcare, Beijing 100176, China

[3] GE Healthcare, Shanghai 201203, China

IDM	Inverse difference moment
K_{ep}	Rate constant
K^{trans}	Volume transfer constant
LAVA	Liver acquisition volume acceleration
NEX	Number of excitations
ROI	Region of interest
TA	Texture analysis
TE	Echo time
TR	Repetition time
V_e	Extravascular extracellular space volume fraction
V_p	Plasma volume fraction

Introduction

Microangiopathy is a key factor in the development of diabetic myopathy; it includes components such as capillary network and endothelial cell dysfunction [1], microvascular barrier injury, increased capillary filtration of albumin [2], and abnormal number of microvessels [3]. The associated physiological signs, including alterations in skeletal muscle structure and function, or reduced metabolic capacity, may cause weakness, increase fatigability, and have a negative impact on insulin sensitivity and processing of glycaemic and lipidemic loads [4]. Diabetic animal models also exhibit muscle wasting and reduced muscular endurance and strength [5, 6]. These effects subsequently lead to the initiation and progression of other diabetic complications. Improving microcirculation via modulation of endothelial dysfunction and induction of angiogenesis [7, 8] has been a potential therapeutic target for diabetic myopathy. Hence, non-invasive quantitative evaluation of microvascular permeability and microarchitectural changes is critical for understanding the pathophysiological mechanisms and to evaluate their curative effects on diabetic skeletal muscle lesions.

However, this non-invasive assessment of skeletal muscle has been methodologically limited. Muscle perfusion encompasses both the rate and distribution of blood flow in the tissue [9]. Arterial spin labelling (ASL), which uses blood as an internal tracer, and dynamic susceptibility contrast (DSC)-MRI, which tracks the distribution of a contrast agent bolus by measuring the effective transverse relaxation rate, are effective tools used to calculate the blood flow [10, 11]. Contrastingly, the use of dynamic contrast-enhanced MRI (DCE-MRI) with the application of an external tracer directly reveals the physiological tissue characteristics (e.g., perfusion and capillary permeability); this is based on kinetic parameters and is performed by fitting the pharmacokinetic models to the concentration curves [12]. It has shown accuracy and feasibility in evaluating the microcirculation in low-perfused healthy skeletal muscle tissue [13, 14], and in the detection of damaged microvascular structures in the skeletal muscle following ischaemia-reperfusion (I/R) injury [15]; it also provides an early and sensitive diagnosis for denervated skeletal muscles [16]. However, few studies have employed DCE-MRI to evaluate diabetic muscle permeability and perfusion [17, 18]. Volume transfer constant (K^{trans}) represents the transfer rate of contrast agents from vessels to the extravascular extracellular space (EES); it provides comprehensive information on microvascular flow, capillary surface area, and permeability, and is the most commonly used parameter to evaluate microvascular permeability in oncological studies. Studies on DCE-MRI of skeletal muscle also showed effectiveness of K^{trans} [15, 16, 19, 20]. Texture analysis (TA) is a potential tool to identify subtle differences in lesion distribution patterns on muscle MRI images [21–23]. Texture features extracted from K^{trans} maps may be useful for analysing lesion perfusion patterns and intralesional heterogeneity, as well as for tumour grading [24] and differentiation [25].

To date, TA of K^{trans} maps obtained from skeletal muscle images has not been reported. Therefore, we aimed to estimate the microvascular permeability and perfusion of skeletal muscle in alloxan-induced diabetic rabbits using quantitative DCE-MRI; we also explored the feasibility of using TA based on K^{trans} map to evaluate subtle structural changes in skeletal muscle in the early stages of diabetes.

Materials and methods

Diabetic rabbit model

All experiments were approved by the Animal Ethics Committee of Wuhan University and the Animal Experiment Centre of Renmin Hospital of Wuhan University. Twenty-four young male Japanese big ear rabbits (weighing 2.8–3.1 kg) were adapted to an adjusted diet plan for 1 week. Fasting blood glucose levels of all rabbits were controlled without exceeding 6.0 mmol/L before preparation of the diabetes mellitus (DM) model. Subsequently, the rabbits were randomly divided into control (n = 10) and diabetic (n = 14) groups, with the latter induced with 5% alloxan monohydrate (Sigma-Aldrich Chemical) dissolved in 0.9% sterile saline, and administered intravenously to the marginal ear vein (100 mg/kg). A successful diabetic rabbit model was defined as the one with blood glucose levels ≥ 14 mmol/L (once) or ≥ 11 mmol/L (twice) at 48 h [26]. Blood glucose levels were weekly monitored in all rabbits for the subsequent 4 weeks until the condition tended toward stability; the levels were measured before MRI examination.

MRI examination

All rabbits were anaesthetised with an injection of 3% pentobarbital sodium (40 mg/kg) via the ear marginal vein [27].

This agent provided fast and deep anaesthesia with a long duration (~ 30 min). The rabbits were imaged at the lumbar level of the multifidus muscle in a 3.0-T MR scanner (Discovery MR750, GE Healthcare) with an 8-channel knee coil after anaesthesia at fixed time points (0, 4, 8, 12, and 16 weeks after verification of a successful diabetic rabbit model). The midline of the intervertebral disc at L6/7 level was selected as the scanning canter. The anatomical images were obtained with axial fast spin-echo T1-weighted sequence (repetition time [TR]/echo time [TE] = 400/9.6 ms; slice thickness = 3.0 mm; field of view [FOV]= 12 cm × 12 cm; matrix = 256 × 256; number of excitations [NEX] = 2) and fast spin-echo T2-weighted anatomic images (TR/TE = 2500/121.7 ms; slice thickness = 3.0 mm; FOV = 12 cm × 12 cm; matrix = 256 × 256; NEX = 4).

DCE-MRI was acquired with liver acquisition volume acceleration (LAVA), using the array spatial sensitivity encoding technique. Pre-contrast LAVA series with variable flip angles used for T1 mapping (TR/TE = 3.5/1.6 ms; slice thickness = 3.0 mm; slice number = 12; FOV = 20 cm × 16 cm; matrix = 256 × 256; flip angles = 9° and 12°) were performed first. Subsequently, dynamic contrast-enhanced sequences were acquired using the LAVA series (flip angle = 10°) with continuous scanning for 35 phases. The temporal resolution of each acquisition was 8 s. The contrast agent gadodiamide (Omniscan; GE Healthcare) was injected via an intravenous catheter placed in the ear marginal vein by a contrast media injector (Medrad Spectris Solaris EP Mobile Mount MR Injection System) at a dose of 0.2 mmol/kg and flow rate of 1.0 mL/s after 2-phase scan as baseline; this procedure was followed by 5 mL saline flush.

Data analysis

Primary DCE-MRI data were analysed using a vendor-offered DCE post-processing software (Omni Kinetics, GE Healthcare). First, 3D non-rigid registration of the 35-phase dynamic enhanced images was performed to reduce respiration and motion artefacts. Second, pre-contrast LAVA series with flip angles of 9° and 12° were used to calculate pixel-wise T1 maps to obtain pre-contrast tissue longitudinal relaxation time T_1 (T_{10}). This measurement would then be used to convert the signal intensity units into units of contrast agent concentration. Then, the corrected 35-phase enhanced images were imported to the software. A dual-compartment extended Tofts linear model was then selected to fit the rabbit muscle. A circular region of interest (ROI) was placed in the centre of the abdominal aorta to obtain the time-concentration curve as the arterial input function (AIF). Each ROI with an area of approximately 40 mm^2 (82 voxels) was placed manually in the ipsilateral multifidus muscle on each image without involvement of subcutaneous fat, fascia, and vertebra. All the ROIs were stacked to a volume of interest. Quantitative permeability parameters including K^{trans}, rate constant (K_{ep}), extravascular extracellular space (EES) volume fraction (V_e), and plasma volume fraction (V_p) (mean value) were calculated. Texture features were extracted automatically from the K^{trans} map, and the number of bins was set at 50. All relevant parameters of the contralateral multifidus muscle were obtained with the same procedure. Two radiologists with more than 5 years of experience in musculoskeletal MR imaging were blinded to the treatment groups and performed all the measurements mentioned above. The mean values of parameters acquired from both examiners were adopted for analysis.

Texture features extracted from the K^{trans} map included histogram parameters (e.g., min, max, median, mean, skewness, and kurtosis) and five commonly used grey level co-occurrence matrix (GLCM) parameters (e.g., energy, entropy, correlation, inverse difference moment [IDM], and contrast). The histogram represents the distribution of pixel intensities in an image [28]. Kurtosis describes the tailedness of the distribution. Skewness measures the asymmetry of the probability distribution. Positive skewness indicates that the distribution is concentrated on the left of the figure. GLCM describes the adjacency relationship between two pixels determined by the spatial distance and direction [29]. Entropy represents the randomness and complexity of intensity values in an image. Energy and IDM reflect the uniformity or homogeneity of intensity value. Correlation measures grey-level linear-dependency between neighbouring resolution units. Contrast calculates the differences in neighbouring pixel values, which indicate the local grey-level variations.

Histological analysis

All rabbits were euthanised with intravenously injected pentobarbital sodium (100 mg/kg) after MRI examination at the 16th week. Samples of the multifidus muscle at L6/7 level of the intervertebral disc were collected, fixed in muscle-specific fixatives, embedded in paraffin, and sliced into 4-μm serial sections perpendicular to the muscle fibres. Sections were stained with haematoxylin-eosin (HE) and labelled with CD31 to measure the muscle fibre mean cross-sectional area (CSA) and capillary-to-fibre (C/F) ratio, respectively. Section images were captured at × 200 magnification using a light microscope (OLYMPUS BX51) with a digital camera; they were then analysed with Image Pro-plus 6.0 software. Four sample fields with approximately 200 muscle fibres were selected from stained sections in each muscle to obtain the CSA [30]. C/F ratio was determined on four separate artefact-free regions of the slice images and calculated as the number of capillaries divided by the number of muscle fibres in these defined areas [31].

Statistical analyses

Normal distribution data are presented as mean ± standard deviation, whereas non-normally distributed data are presented as median (25th–75th percentiles). The two-sample *t* test (data with a normal distribution and equal homogeneity of variance) or Mann-Whitney *U* test was used to evaluate differences in CSA, C/F ratio, permeability parameters, and texture parameters between the groups at the same time point. Repeated measures analysis of variance (data with normal distribution and Mauchly's test of sphericity with Greenhouse-Geisser or Huynh-Feldt correction if necessary) or the Friedman test was applied to assess the differences in these parameters at different time points in the same group, followed by Bonferroni correction for post hoc pairwise comparisons. Pearson correlations were used to estimate the correlations between CSA and C/F ratio and permeability parameters. All statistical analyses were performed with SPSS 17.0 Windows Student Version statistics software (IBM). $p < 0.05$ was considered statistically significant.

Results

In the diabetic group, two animals failed to maintain a hyperglycaemic state while two others died from poor health condition. The failure and mortality rate were 14.3%, respectively. In the control group, one animal died because of an anaesthetic accident, and another died of unknown causes. These six rabbits were excluded from the experiment. The successfully induced diabetic rabbits exhibited weight loss and tissue wasting over time, as well as decreased activity and reduced flexibility.

Axial T1WI images revealed significantly reduced multifidus muscle and subcutaneous fat areas in the diabetic group at the 16th week relative to these measures in week 0. There were no obvious changes in control group over time (Fig. 1).

The control group showed no significant differences in permeability parameters over time (Table 1). In the diabetic group, K^{trans} and K_{ep} were significantly higher at the 8th week than the baseline, and they respectively decreased significantly at the 16th and 12th weeks compared to the 8th week. Additionally, V_e increased while V_p decreased from the 8th week. Apart from the baseline and at the 4th week, K^{trans}, K_{ep}, and V_e were higher, while the V_p was lower at each time point in the diabetic group than in the control group (Table 2; Figs. 2 and 3). Additionally, DCE-MRI pharmacokinetic parameter maps reflected a higher permeability and poor perfusion of muscles in the diabetic group at the 16th week (Fig. 2).

All the texture parameters in the control group were not significantly different (Table 1). In the diabetic group, the skewness began to decrease significantly at the 4th week and increased significantly at the 16th week. From the 8th week, median K^{trans}, mean K^{trans}, and entropy increased significantly, whereas IDM decreased. The energy also decreased while the contrast increased significantly in the diabetic group, only at the 8th week (Tables 3 and 4).

Cross-sections of HE-stained multifidus muscles revealed muscle fibre atrophy and widened interstitial spaces between fibres. CD31-Stained muscle fibres also exhibited sparse microvessel distribution in the diabetic group at the 16th week (Fig. 4). CSA and C/F were decreased in the diabetic group (3332.823 ± 532.908 μm^2, 0.580 ± 0.060) compared to those in the control group (5841.718 ± 306.501 μm^2, 1.035 ± 0.072) (t = − 11.802 and − 14.650, respectively; $p < 0.001$) (Fig. 5). CSA was negatively correlated with K^{trans} and V_e, and positively correlated with V_p (r = − 0.821, − 0.823, and 0.826, respectively, $p < 0.05$). Furthermore, C/F was negatively correlated with K^{trans}, K_{ep}, and V_e, and positively correlated with V_p (r = − 0.854, − 0.503, − 0.768, and 0.908, respectively; $p < 0.05$).

Discussion

To our best knowledge, this is the first study to estimate the microcirculation and structural changes in skeletal muscle in alloxan-induced diabetic rabbits using permeability parameters of DCE-MRI and texture features extracted from K^{trans} maps. We observed that microvascular permeability, CSA, and C/F ratio of the multifidus muscle were altered in DM. The permeability parameters were correlated with CSA and C/F ratio. K^{trans} map-based texture parameters reflected these microarchitectural changes in diabetic skeletal muscles.

The multifidus muscle was selected for two reasons. First, it is a distinguishable anatomical landmark and pathologic specimen. Second, it plays a crucial role in maintaining the stability of the lumbosacral spine, which is closely related to low back pain, denervation, and spinal deformities [32]. Microvascular endothelium barrier dysfunction is a classic feature of DM in the early stage due to glucose toxicity and inflammatory responses. Metabolic toxicity may cause skeletal muscle pericyte dysfunction and loss, which in turn diminishes its supportive–protective effect on capillary endothelial cells before capillary loss. These reactions may result in ultrastructural remodelling in microvascular beds, and consequent plasma leakage in various tissues, including skeletal muscle [33, 34]. Thus, microvascular permeability is altered in diabetic muscles. Our study revealed increased K^{trans} and K_{ep} at the 8th week in the diabetic group. Ganesh et al [15] have attributed the increased K^{trans} of skeletal muscle to the loss of endothelial integrity in an I/R injury model. Likewise, our study's findings suggest hyperpermeability and reflect endothelial barrier injury in the early stage of diabetes. We also observed a decreasing trend of K^{trans} and K_{ep} in the diabetic

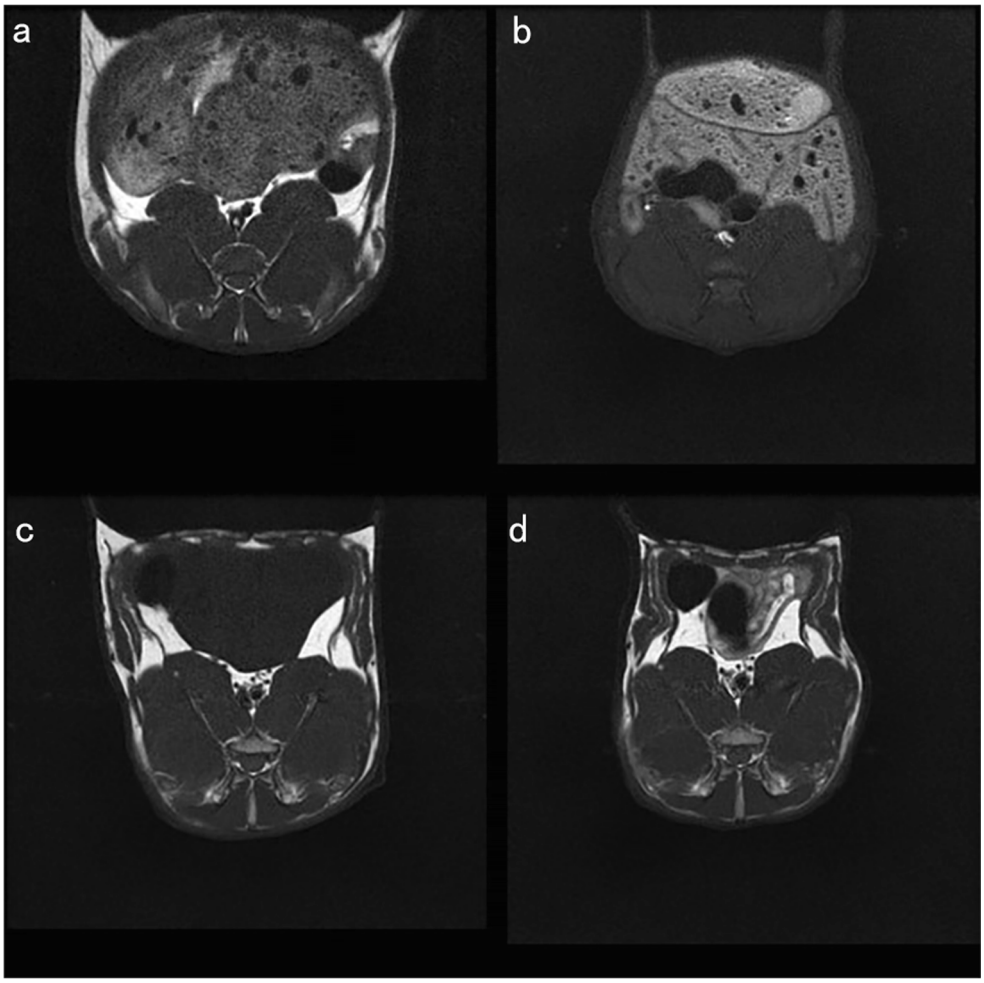

Fig. 1 Axial T1WI images of the diabetic and control groups. **a** Subcutaneous fat and multifidus muscles are clearly visible in the diabetic group at week 0, (**b**) but are significantly reduced at the 16th week. There are no obvious changes in the control group between (**c**) week 0 and (**d**) the 16th week

group. These effects may be related to abnormal perfusion. Decreased perfusion in diabetic muscles has been supported by evidence from studies of adequate imaging techniques and other methods, such as decreased initial area under the signal intensity-time curve value over the first 60 s ($IAUC_{60}$) on DCE-MRI [18], reduced perfusion ratio on laser Doppler perfusion imaging [35], reduced blood flow on ASL [10], and reduced video intensity on contrast-enhanced ultrasound (CEU) [36] in diabetic animals and patients. Wang et al [17] demonstrated that diabetic patients experienced severe ischaemic damage displayed significantly lower K^{trans} values in the tibialis anterior muscles. In this condition, reduced perfusion may have induced a decrease in K^{trans}. Conversely, our study focused on animal models of DM in the early stages; hence, the inconsistency may be attributed to differences in disease duration.

V_p represents the fractional volume of plasma per unit volume of tissue [12]. To this end, the reduced V_p values in our study may reflect decreased perfusion in the diabetic group, consistent with previous studies. Decreased C/F ratio signifies sparse capillaries between the diabetic muscle fibres. This factor may explain the reduction in V_p, considering the strong positive correlation between factors. Our study revealed increased V_e in the diabetic group from the 8th week, suggesting an expanded EES; this corresponded to the enlarged interstitial spaces between diabetic muscle fibres as shown on HE staining. Additionally, decreased CSA of diabetic muscles was observed, which is consistent with previous findings [37]. Our study also revealed a strong negative correlation between CSA and V_e, demonstrating that muscle fibre atrophy may induce an increase in V_e as EES expands. Therefore, V_e may be useful for assessing muscle atrophy.

In this study, median K^{trans} was significantly increased in the diabetic group at the 8th week; as with mean K^{trans}, this suggested greater permeability. Skewness has recently been investigated in several studies. Shukla-Dave et al [38] reported that skewness of K^{trans} was a strong predictor of progression-free survival and overall survival in head and neck squamous cell carcinoma patients with stage IV nodal disease. Just [39] also demonstrated that hypoxic and necrotic regions increased asymmetric distributions (skewness) of K^{trans} and K_{ep} in DCE-MRI, indicating poor perfusion within tumours. In our study, both groups showed positive skewness of K^{trans} values; however, a lower skewness was observed in the diabetic group

Table 1 Repeated measure of permeability and texture parameters in diabetic and control groups

	Diabetic group		Control group	
	F	*p* value	*F*	*p* value
K^{trans}	40.696	< 0.001	0.304	0.873
K_{ep}	15.516	< 0.001	0.176	0.949
V_e	18.482	< 0.001	0.314	0.867
V_p	64.383	< 0.001	0.729	0.579
min	-	0.929	-	0.997
max	-	0.994	-	0.914
Median	24.779	< 0.001	0.065	0.992
Skewness	56.98	< 0.001	0.378	0.822
Kurtosis	0.923	0.461	0.644	0.635
Energy	-	0.030	-	0.894
Entropy	16.672	< 0.001	0.282	0.887
Correlation	2.295	0.121	0.169	0.953
IDM	23.902	< 0.001	0.326	0.858
Contrast	6.390	0.001	0.367	0.830

- represents Friedman test

K^{trans}, volume transfer constant; K_{ep}, rate constant; V_e, extravascular extracellular space volume fraction; V_p, plasma volume fraction; *IDM*, inverse difference moment

Table 2 Permeability parameters in the diabetic and control groups at each time point

Time point	Diabetic group	Control group	*t*(*Z*)	*p* value
K^{trans} (min^{-1})				
Week 0	1.381 ± 0.279	1.333 ± 0.219	0.403	0.693
Week 4	1.516 ± 0.207	1.432 ± 0.207	0.849	0.409
Week 8	2.809 ± 0.345*	1.378 ± 0.251	9.799	< 0.001#
Week 12	2.504 ± 0.493*	1.430 ± 0.262	5.537	< 0.001#
Week 16	2.422 ± 0.300*†	1.368 ± 0.213	8.368	< 0.001#
K_{ep} (min^{-1})				
Week 0	1.681 ± 0.236	1.625 ± 0.256	0.476	0.641
Week 4	1.853 ± 0.249	1.603 ± 0.258	2.090	0.053
Week 8	2.478 ± 0.344*	1.652 ± 0.273	5.534	< 0.001#
Week 12	2.102 ± 0.378*†	1.707 ± 0.292	2.425	0.027#
Week 16	2.061 ± 0.352*†	1.672 ± 0.298	2.484	0.024#
V_e				
Week 0	0.649 ± 0.129	0.618 ± 0.132	0.498	0.626
Week 4	0.657 ± 0.139	0.609 ± 0.121	0.771	0.452
Week 8	0.891 ± 0.054*	0.573 ± 0.124	7.344	< 0.001#
Week 12	0.874 ± 0.070*	0.558 ± 0.130	6.620	< 0.001#
Week 16	0.909 ± 0.028*	0.589 ± 0.158	− 3.554 [a]	< 0.001#
V_p				
Week 0	0.412 ± 0.123	0.451 ± 0.115	− 0.693	0.498
Week 4	0.367 ± 0.085	0.447 ± 0.126	− 1.595	0.130
Week 8	0.090 ± 0.022*	0.501 ± 0.123	− 3.554 [a]	< 0.001#
Week 12	0.104 ± 0.023*	0.526 ± 0.146	− 3.554 [a]	< 0.001#
Week 16	0.104 ± 0.016*	0.505 ± 0.137	− 3.554 [a]	< 0.001#

Data are mean ± standard deviation (accord with normal distribution) or median (25th–75th percentiles)

*$p < 0.05$ versus week 0 in the same group

†$p < 0.05$ versus week 8 in the same group

#$p < 0.05$ for the diabetic group versus the control group at the same time point

[a] Represents *Z* value of Mann-Whitney *U* test

K^{trans}, volume transfer constant; K_{ep}, rate constant; V_e, extravascular extracellular space volume fraction; V_p, plasma volume fraction

from the 4th week, although this group had relatively poor perfusion. A possible explanation is that there were no areas of obvious cystoid variation and necrosis within diabetic skeletal muscle in our study, and the distribution of K^{trans} tended to higher intensity values than those of the control group, as permeability increased. This also indicates that skewness of K^{trans} may have advantages for estimating the permeability of diabetic muscles at an early stage.

Energy (angular second moment, ASM), entropy, correlation, IDM, and contrast are frequently used for evaluating tumour heterogeneity; they have also been applied in the evaluation of skeletal muscles. A longitudinal study demonstrated that the shortened walking distance of patients with lumbar spinal stenosis was associated with entropy based on axial T2W TSE images of the paraspinal muscle [22]. Watanabe et al [40] observed decreased IDM and ASM in sonograms of aging quadriceps femoris muscle. Mahmoud-Ghoneim et al [41] reported that ASM and entropy could discriminate muscle conditions of normal, atrophy, and regeneration in rats, which were related to abnormal modifications in the mean CSA of type 2 fibres. In another study, contrast and entropy based on T2WI could identify different texture distribution of leg muscle groups in various mouse models of muscular dystrophies; this was related to degenerating and regenerating muscle cells, inflammatory infiltrates, and differential distribution of fibrosis [21]. These GLCM parameters demonstrate a potential value in identifying subtle changes in skeletal muscle microstructure, and associations with pathology increase the robustness of these observations.

Our study revealed higher entropy and lower IDM in the diabetic group from the 8th week, indicating increased complexity and irregularity of K^{trans} map texture. This may be explained by histological findings. Amin et al [42] observed markedly increased interstitial connective tissue around blood vessels and muscle fibres, as well as ultrastructural modifications such as disrupted sarcomere organisation, swollen mitochondria, and lipid droplet infiltration in diabetic skeletal muscles. Our results revealed sparsely distributed microvessels and atrophic muscle fibres with enlarged interstitial spaces. The axial T1WI images in our study also showed muscular atrophy. These factors may have contributed to uneven

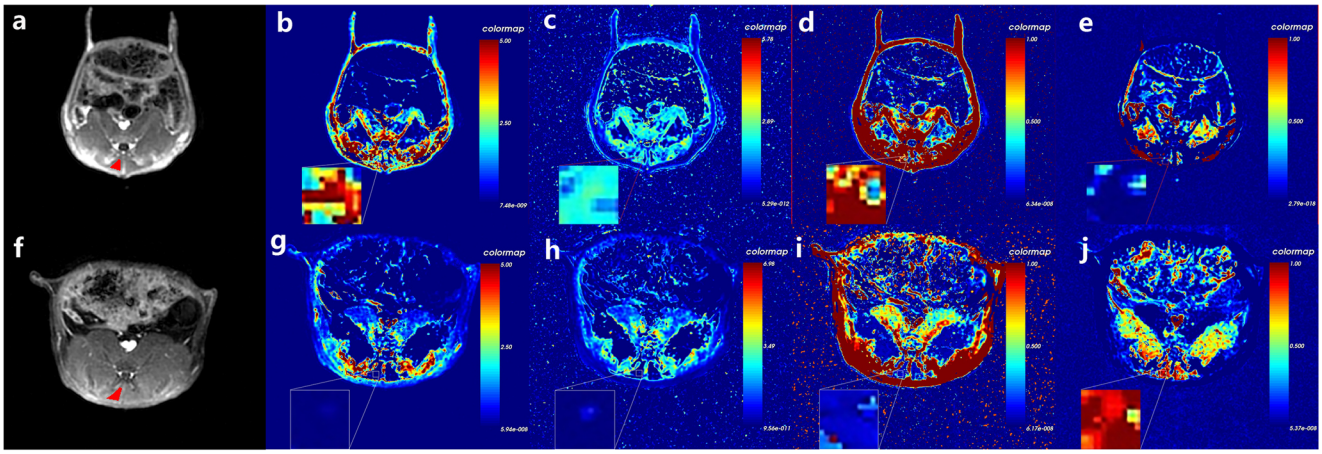

Fig. 2 Post-contrast axial T1WI images and pharmacokinetic maps in diabetic and control groups at the 16th week. **a** shows post-contrast axial T1WI images of the multifidus muscle of the diabetic group. The red area indicates an ROI on the right side. **b** K^{trans}, (**c**) K_{ep}, (**d**) V_e, and (**e**) V_p maps are shown, with values of 2.096 min^{-1}, 1.807 min^{-1}, 0.848, and 0.133, respectively. **f** shows post-contrast axial T1WI images of the multifidus muscle of the control group. The red area indicates an ROI on the right side. **g** K^{trans}, (**h**) K_{ep}, (**i**) V_e, and (**j**) V_p maps are shown, with values of 1.045 min^{-1}, 1.282 min^{-1}, 0.381, and 0.639, respectively. A zoom of the multifidus muscle is shown in the bottom left corner of each pharmacokinetic map

distribution of contrast medium in diabetic muscles, resulting in increased complexity and local variability in image texture. Contrast significantly increased while energy decreased in the diabetic group only at the 8th week, reflecting differences in grey levels of adjacent pixels and higher inhomogeneity of K^{trans} map at this time point. These findings suggested that

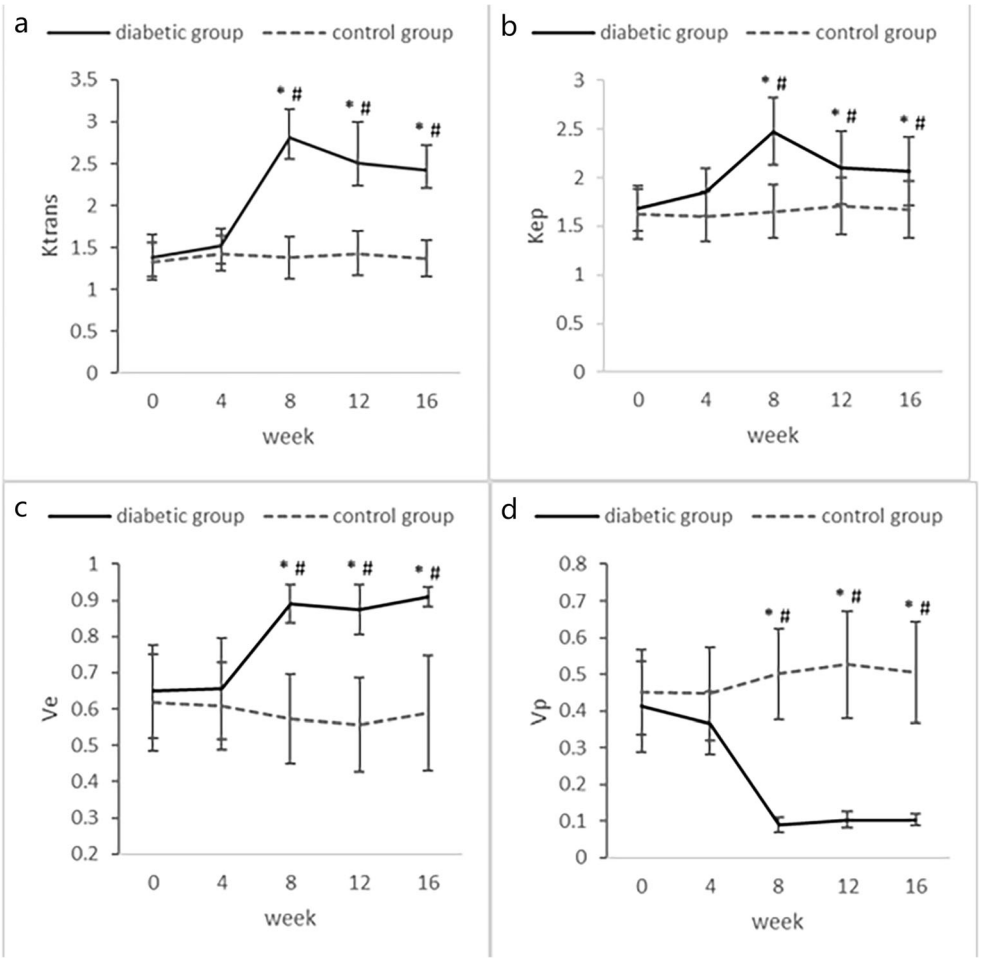

Fig. 3 Permeability parameters of the diabetic and control groups. All parameters were significantly different between the diabetic group (solid line) and control group (dotted line) at the 8th, 12th, and 16th weeks ($^{\#}p < 0.05$). K^{trans} and K_{ep} were increased at the 8th week and subsequently exhibited a decreasing trend. V_e was increased whereas V_p was decreased at the 8th week, after which they were stable in the diabetic group ($^{*}p < 0.05$)

Table 3 K^{trans} histogram parameters in the diabetic and control groups at each time point

Time point	Diabetic group	Control group	$t(Z)$	p value
min				
Week 0	0.000 (0.000,0.034)	0.000 (0.000,0.027)	− 0.635 [a]	0.633
Week 4	0.000 (0.000,0.044)	0.000 (0.000,0.046)	− 0.265 [a]	0.829
Week 8	0.000 (0.000,0.025)	0.000 (0.000,0.013)	− 0.337 [a]	0.829
Week 12	0.000 (0.000,0.033)	0.000 (0.000,0.030)	− 0.202 [a]	0.897
Week 16	0.000 (0.000,0.022)	0.000 (0.000,0.023)	− 0.101 [a]	0.965
max				
Week 0	5.000 (4.191,5.000)	5.000 (4.156,5.000)	− 0.159 [a]	0.897
Week 4	5.000 (4.425,5.000)	5.000 (3.937,5.000)	− 0.159 [a]	0.897
Week 8	5.000 (4.221,5.000)	5.000 (3.997,5.000)	− 0.265 [a]	0.829
Week 12	5.000 (4.189,5.000)	5.000 (4.466,5.000)	− 0.112 [a]	0.965
Week 16	5.000 (4.221,5.000)	5.000 (4.359,5.000)	− 0.265 [a]	0.829
Median				
Week 0	1.114 ± 0.324	1.081 ± 0.360	0.206	0.839
Week 4	1.187 ± 0.400	1.117 ± 0.347	0.390	0.702
Week 8	2.761 ± 0.605*	1.075 ± 0.337	7.031	< 0.001#
Week 12	2.458 ± 0.575*	1.062 ± 0.340	6.049	< 0.001#
Week 16	2.371 ± 0.480*	1.133 ± 0.344	6.132	< 0.001#
Mean				
Week 0	1.381 ± 0.279	1.333 ± 0.219	0.403	0.693
Week 4	1.516 ± 0.207	1.432 ± 0.207	0.849	0.409
Week 8	2.809 ± 0.345*	1.378 ± 0.251	9.799	< 0.001#
Week 12	2.504 ± 0.493*	1.430 ± 0.262	5.537	< 0.001#
Week 16	2.422 ± 0.300*†	1.368 ± 0.213	8.368	< 0.001#
Skewness				
Week 0	1.082 ± 0.286	1.018 ± 0.274	0.480	0.638
Week 4	0.748 ± 0.281*	1.066 ± 0.293	− 2.344	0.032#
Week 8	0.055 ± 0.436*	0.993 ± 0.264	− 5.341	< 0.001#
Week 12	0.184 ± 0.490*	0.968 ± 0.272	− 4.035	0.001#
Week 16	0.345 ± 0.329*†	1.104 ± 0.301	− 5.051	< 0.001#
Kurtosis				
Week 0	1.120 ± 0.847	1.308 ± 0.864	− 0.463	0.650
Week 4	1.029 ± 0.878	1.252 ± 0.892	− 0.533	0.602
Week 8	0.571 ± 0.561	0.952 ± 0.801	− 1.188	0.252
Week 12	0.785 ± 0.571	0.929 ± 0.796	− 0.444	0.663
Week 16	0.811 ± 0.594	0.894 ± 0.745	− 0.264	0.796

Data are mean ± standard deviation (accord with normal distribution) or median (25th–75th percentiles)

* $p < 0.05$ versus week 0 in the same group

† $p < 0.05$ versus week 8 in the same group

# $p < 0.05$ for the diabetic group versus the control group at the same time point

[a] Represents Z value of Mann-Whitney U test

entropy and IDM might be more sensitive than other GLCM parameters for detecting altered microarchitecture in diabetic muscles.

There are several limitations to this study. First, the progression of diabetes-induced animals was only observed for 16 weeks; therefore, understanding complete temporal variations in permeability of diabetic muscles requires further study. Second, our study did not investigate clinical signs of myopathy and microvascular pathology. More pathological markers of myopathy, such as blood flow/perfusion obtained by DSC or ASL MRI, MR spectroscopy, and functional parameters (e.g., force and fatigability), are needed to discern

Table 4 K^{trans} grey level co-occurrence matrix parameters in the diabetic and control groups at each time point

Time point	Diabetic group	Control group	*t*(*Z*)	*p* value
Energy ($\times10^{-3}$)				
Week 0	4.940 (4.200,23.360)	7.510 (4.260,36.850)	− 0.444 [a]	0.696
Week 4	8.720 (5.950,24.690)	10.020 (5.890,32.460)	− 0.178 [a]	0.897
Week 8	3.470 (2.700,8.710)	9.310 (5.080,29.630)	− 2.310 [a]	0.021#
Week 12	5.510 (3.870,16.280)	10.290 (5.350,27.510)	− 1.244 [a]	0.237
Week 16	3.840 (2.810,9.030)	9.600 (4.000,38.300)	− 1.777 [a]	0.083
Entropy				
Week 0	7.852 ± 0.768	7.775 ± 0.607	0.231	0.820
Week 4	7.900 ± 0.587	7.603 ± 0.725	0.962	0.350
Week 8	8.930 ± 0.164*	7.711 ± 0.991	− 2.843 [a]	0.003#
Week 12	8.545 ± 0.493*	7.415 ± 1.116	− 2.399 [a]	0.016#
Week 16	8.701 ± 0.465*	7.530 ± 1.020	3.250	0.005#
Correlation ($\times10^{-3}$)				
Week 0	13.590 ± 5.765	13.750 ± 9.050	− 0.046	0.964
Week 4	13.900 ± 7.137	12.200 ± 5.944	0.541	0.596
Week 8	8.340 ± 3.547	11.040 ± 6.147	− 1.168	0.260
Week 12	9.240 ± 4.108	12.810 ± 7.090	− 1.338	0.199
Week 16	9.180 ± 4.585	12.110 ± 5.735	− 1.206	0.245
IDM				
Week 0	0.353 ± 0.070	0.350 ± 0.092	0.099	0.922
Week 4	0.329 ± 0.047	0.369 ± 0.071	− 1.438	0.170
Week 8	0.233 ± 0.032*	0.357 ± 0.092	− 2.754 [a]	0.004#
Week 12	0.277 ± 0.029*	0.391 ± 0.117	− 2.310 [a]	0.021#
Week 16	0.246 ± 0.045*	0.369 ± 0.105	− 3.339	0.004#
Contrast ($\times10^{-3}$)				
Week 0	10.110 ± 3.412	10.570 ± 3.334	− 0.283	0.780
Week 4	11.670 ± 6.942	13.420 ± 7.382	− 0.517	0.612
Week 8	18.000 ± 3.571*	12.750 ± 5.542	2.437	0.027#
Week 12	16.980 ± 6.133	12.390 ± 6.623	1.524	0.147
Week 16	16.450 ± 6.900	13.020 ± 6.188	1.097	0.289

Data are mean ± standard deviation (accord with normal distribution) or median (25th–75th percentiles)

*$p < 0.05$ versus week 0 in the same group

† $p < 0.05$ versus week 8 in the same group

# $p < 0.05$ for the diabetic group versus the control group at the same time point

[a] Represents *Z* value of Mann-Whitney *U* test

IDM, inverse difference moment

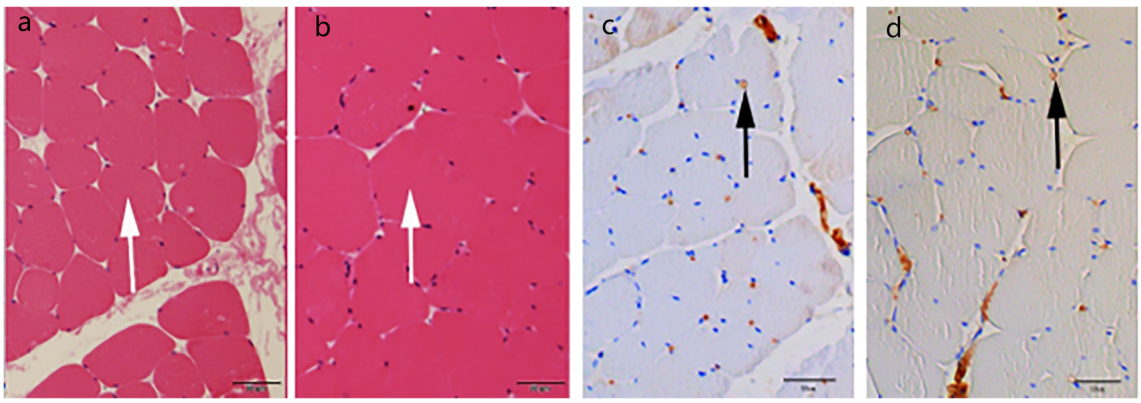

Fig. 4 Transverse histologic sections of multifidus muscle fibres. The muscle fibres (white arrow) demonstrated atrophy in the (**a**) diabetic group compared to that in the (**b**) control group (haematoxylin-eosin stain; original magnification, ×200). Microvessels (black arrow) among the muscle fibres were sparser in the (**c**) diabetic group than in the (**d**) control group (CD31 stain; original magnification, ×200)

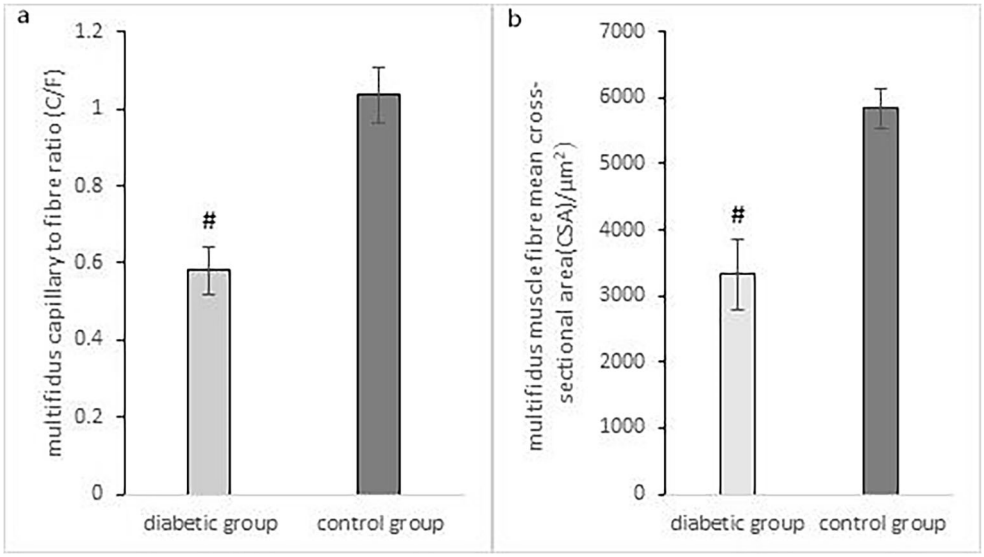

Fig. 5 **a** Mean cross-sectional area (CSA) and (**b**) capillary-to-fibre ratio (C/F) of multifidus muscle fibres in diabetic and control groups. CSA and C/F were decreased in the diabetic group compared to those in the control group ($^{\#}p < 0.05$)

subtle changes in skeletal muscle features and investigate the confounding factors of microvascular permeability and perfusion. Third, the low temporal resolution (8 s) may lead to overestimations of the V_p value. In addition, the sum of V_p and V_e in few rabbits showed values slightly greater than 1, which might be due to a computational bias, when a pharmacokinetic model based on a database of humans was used on rabbits. A multi-compartment pharmacokinetic model might be a more suitable pharmacokinetic model for evaluating the multifidus muscle of rabbits. Despite this, differences between the diabetic and control groups indicate that V_p and V_e are promising parameters with which to estimate the blood supply in the skeletal muscle. Finally, a small sample size was used. Definitive conclusions on texture features of diabetic skeletal muscle should be confirmed by using larger samples.

In conclusion, quantitative DCE-MRI can be used to evaluate microvascular permeability and perfusion of diabetic skeletal muscles; TA based on K^{trans} maps can identify microarchitectural modifications in diabetic skeletal muscle at early stages.

Acknowledgements Dr. Ling Ma gave constructive suggestions on the revision of this article.

Funding This study was supported by the National Natural Science Foundation of China (Grant Numbers 81871332 and 81801670).

Compliance with Ethical Standards

Guarantor The scientific guarantor of this publication is Yunfei Zha.

Conflict of interest Two of the authors of this manuscript (Weiyin Vivian Liu and Huan Liu) are employees of GE Healthcare. The remaining authors declare no relationships with any companies whose products or services may be related to the subject matter of the article.

Statistics and biometry No complex statistical methods were necessary for this paper.

Informed consent Approval from the institutional animal care committee was obtained.

Ethical approval Institutional Review Board approval was obtained.

Methodology
- prospective
- experimental
- performed at one institution

References

1. Coleman SK, Rebalka IA, D'Souza DM, Hawke TJ (2015) Skeletal muscle as a therapeutic target for delaying type 1 diabetic complications. World J Diabetes 6:1323–1336
2. Cohen-Boulakia F, Valensi PE, Boulahdour H et al (2000) In vivo sequential study of skeletal muscle capillary permeability in diabetic rats: effect of anthocyanosides. Metabolism 49:880–885
3. Groen BB, Hamer HM, Snijders T et al (2014) Skeletal muscle capillary density and microvascular function are compromised with aging and type 2 diabetes. J Appl Physiol (1985) 116:998–1005
4. Monaco CMF, Perry CGR, Hawke TJ (2017) Diabetic myopathy: current molecular understanding of this novel neuromuscular disorder. Curr Opin Neurol 30:545–552
5. Chiu CY, Yang RS, Sheu ML et al (2016) Advanced glycation end-products induce skeletal muscle atrophy and dysfunction in diabetic mice via a RAGE-mediated, AMPK-down-regulated, Akt pathway. J Pathol 238:470–482
6. Tseng YT, Chang WH, Lin CC, Chang FR, Wu PC, Lo YC (2019) Protective effects of Liuwei dihuang water extracts on diabetic muscle atrophy. Phytomedicine 53:96–106
7. You J, Sun J, Ma T et al (2017) Curcumin induces therapeutic angiogenesis in a diabetic mouse hindlimb ischemia model via modulating the function of endothelial progenitor cells. Stem Cell Res Ther 8:182

8. Fromer MW, Chang S, Hagaman ALR et al (2018) The endothelial cell secretome as a novel treatment to prime adipose-derived stem cells for improved wound healing in diabetes. J Vasc Surg 68:234–244
9. Barrett EJ, Rattigan S (2012) Muscle perfusion: its measurement and role in metabolic regulation. Diabetes 61:2661–2668
10. Edalati M, Hastings MK, Muccigrosso D et al (2019) Intravenous contrast-free standardized exercise perfusion imaging in diabetic feet with ulcers. J Magn Reson Imaging 50:474–480
11. Rissanen TT, Korpisalo P, Markkanen JE et al (2005) Blood flow remodels growing vasculature during vascular endothelial growth factor gene therapy and determines between capillary arterialization and sprouting angiogenesis. Circulation 112:3937–3946
12. Khalifa F, Soliman A, El-Baz A et al (2014) Models and methods for analyzing DCE-MRI: a review. Med Phys 41:124301
13. Hindel S, Sohner A, Maass M et al (2017) Validation of blood volume fraction quantification with 3D gradient echo dynamic contrast-enhanced magnetic resonance imaging in porcine skeletal muscle. PLoS One 12:e0170841
14. Hindel S, Sohner A, Maa M et al (2017) Validation of interstitial fractional volume quantification by using dynamic contrast-enhanced magnetic resonance imaging in porcine skeletal muscles. Invest Radiol 52:66–73
15. Ganesh T, Zakher E, Estrada M, Cheng HM (2019) Assessment of microvascular dysfunction in acute limb ischemia-reperfusion injury. J Magn Reson Imaging 49:1174–1185
16. Qi L, Xu L, Wang WT et al (2019) Dynamic contrast-enhanced magnetic resonance imaging in denervated skeletal muscle: experimental study in rabbits. PLoS One 14:e0215069
17. Wang J, Li YH, Li MH, Zhao JG, Bao YQ, Zhou J (2011) Use of dynamic contrast-enhanced magnetic resonance imaging to evaluate the microcirculation of lower extremity muscles in patients with type 2 diabetes. Diabet Med 28:618–621
18. Kashiwagi Y, Nodaira M, Amitani M, Murase K, Abe K (2012) Assessment of peripheral tissue perfusion disorder in streptozotocin-induced diabetic rats using dynamic contrast-enhanced MRI. Magn Reson Imaging 30:254–260
19. Wright KL, Seiberlich N, Jesberger JA et al (2013) Simultaneous magnetic resonance angiography and perfusion (MRAP) measurement: initial application in lower extremity skeletal muscle. J Magn Reson Imaging 38:1237–1244
20. Jaspers K, Leiner T, Dijkstra P et al (2010) Optimized pharmacokinetic modeling for the detection of perfusion differences in skeletal muscle with DCE-MRI: effect of contrast agent size. Med Phys 37:5746–5755
21. Martins-Bach AB, Malheiros J, Matot B et al (2015) Quantitative T2 combined with texture analysis of nuclear magnetic resonance images identify different degrees of muscle involvement in three mouse models of muscle dystrophy: mdx, Largemyd and mdx/Largemyd. PLoS One 10:e0117835
22. Mannil M, Burgstaller JM, Thanabalasingam A et al (2018) Texture analysis of paraspinal musculature in MRI of the lumbar spine: analysis of the lumbar stenosis outcome study (LSOS) data. Skeletal Radiol 47:947–954
23. Nketiah G, Savio S, Dastidar P, Nikander R, Eskola H, Sievanen H (2015) Detection of exercise load-associated differences in hip muscles by texture analysis. Scand J Med Sci Sports 25:428–434
24. Xie T, Chen X, Fang J et al (2018) Textural features of dynamic contrast-enhanced MRI derived model-free and model-based parameter maps in glioma grading. J Magn Reson Imaging 47:1099–1111
25. Sun K, Zhu H, Chai W et al (2020) Whole-lesion histogram and texture analyses of breast lesions on inline quantitative DCE mapping with CAIPIRINHA-Dixon-TWIST-VIBE. Eur Radiol 30:57–65
26. Liu T, Zhao H, Li J, Korantzopoulos P, Li G (2014) Rosiglitazone attenuates atrial structural remodeling and atrial fibrillation promotion in alloxan-induced diabetic rabbits. Cardiovasc Ther 32:178–183
27. Mutolo D, Cinelli E, Bongianni F, Pantaleo T (2014) Inhibitory control of the cough reflex by galanin receptors in the caudal nucleus tractus solitarii of the rabbit. Am J Physiol Regul Integr Comp Physiol 307:R1358–R1367
28. Alobaidli S, McQuaid S, South C, Prakash V, Evans P, Nisbet A (2014) The role of texture analysis in imaging as an outcome predictor and potential tool in radiotherapy treatment planning. Br J Radiol 87:20140369
29. Bino SV, Unnikrishnan A, Balakrishnan K (2012) Grey level co-occurrence matrices: generalisation and some new features. Int J Comput Sci Eng Inf 2:151–157
30. Battistuzzo CR, Rank MM, Flynn JR et al (2017) Effects of treadmill training on hindlimb muscles of spinal cord-injured mice. Muscle Nerve 55:232–242
31. Trappe TA, Ratchford SM, Brower BE et al (2016) COX inhibitor influence on skeletal muscle fiber size and metabolic adaptations to resistance exercise in older adults. J Gerontol A Biol Sci Med Sci 71:1289–1294
32. Zhi-Jun H, Wen-Bin X, Shuai C et al (2014) Accuracy of magnetic resonance imaging signal intensity ratio measurements in the evaluation of multifidus muscle injury and atrophy relative to that of histological examinations. Spine (Phila Pa 1976) 39:E623–E629
33. Yuan SY, Breslin JW, Perrin R et al (2007) Microvascular permeability in diabetes and insulin resistance. Microcirculation 14:363–373
34. Hayden MR, Yang Y, Habibi J, Bagree SV, Sowers JR (2010) Pericytopathy: oxidative stress and impaired cellular longevity in the pancreas and skeletal muscle in metabolic syndrome and type 2 diabetes. Oxid Med Cell Longev 3:290–303
35. Hansen LM, Gupta D, Joseph G, Weiss D, Taylor WR (2017) The receptor for advanced glycation end products impairs collateral formation in both diabetic and non-diabetic mice. Lab Invest 97:34–42
36. Irace C, Messiniti V, Tassone B, Cortese C, Barrett EJ, Gnasso A (2017) Evidence for congruent impairment in micro and macrovascular function in type 1 diabetes. PLoS One 12:e0187525
37. Kemmochi Y, Ohta T, Motohashi Y et al (2018) Pathophysiological analyses of skeletal muscle in obese type 2 diabetes SDT fatty rats. J Toxicol Pathol 31:113–123
38. Shukla-Dave A, Lee NY, Jansen JF et al (2012) Dynamic contrast-enhanced magnetic resonance imaging as a predictor of outcome in head-and-neck squamous cell carcinoma patients with nodal metastases. Int J Radiat Oncol Biol Phys 82:1837–1844
39. Just N (2014) Improving tumour heterogeneity MRI assessment with histograms. Br J Cancer 111:2205–2213
40. Watanabe T, Murakami H, Fukuoka D et al (2017) Quantitative sonographic assessment of the quadriceps femoris muscle in healthy Japanese adults. J Ultrasound Med 36:1383–1395
41. Mahmoud-Ghoneim D, Cherel Y, Lemaire L, de Certaines JD, Maniere A (2006) Texture analysis of magnetic resonance images of rat muscles during atrophy and regeneration. Magn Reson Imaging 24:167–171
42. Amin SN, Hussein UK, Yassa HD, Hassan SS, Rashed LA (2018) Synergistic actions of vitamin D and metformin on skeletal muscles and insulin resistance of type 2 diabetic rats. J Cell Physiol 233:5768–5779